Timing studies on *RXTE* observations of SAX J2103.5+4545

A. Baykal,[1][*] S. Ç. İnam,[2][*] M. J. Stark,[3][*] C. M. Heffner,[3,4][*] A. E. Erkoca[5][*]
and J. H. Swank[6][*]

[1]*Physics Department, Middle East Technical University, 06531 Ankara, Turkey*

[2]*Department of Electrical and Electronics Engineering, Başkent University, 06530 Ankara, Turkey*

[3]*Lafayette College, Easton, PA 18042, USA*

[4]*Department of Physics, University of California, Riverside, CA 92521, USA*

[5]*Department of Physics, University of Arizona, Tucson, AZ 85721, USA*

[6]*NASA Goddard Space Flight Centre, Greenbelt, MD 20771, USA*

ABSTRACT

SAX J2103.5+4545 has been continuously monitored for $\sim$900 d by the *Rossi X-ray Timing Explorer* (*RXTE*) since its outburst in 2002 July. Using these observations and previous archival *RXTE* observations of SAX J2103.5+4545, we refined the binary orbital parameters and find the new orbital period as $P = (12.665\,36 \pm 0.000\,88)$ d and the eccentricity as 0.4055 ± 0.0032. With these new orbital parameters, we constructed the pulse frequency and pulse frequency derivative histories of the pulsar and confirmed the correlation between X-ray flux and pulse frequency derivative presented by Baykal, Stark & Swank. We constructed the power spectra for the fluctuations of pulse frequency derivatives and found that the power-law index of the noise spectra is 2.13 ± 0.6. The power-law index is consistent with random walk in pulse frequency derivative and is the steepest among the HMXRBs. X-ray spectra analysis confirmed the inverse correlation trend between power-law index and X-ray flux found by Baykal et al.

Key words: accretion, accretion discs – stars: neutron – pulsars: individual: SAX J2103.5+4545 – X-rays: binaries.

1 INTRODUCTION

The transient X-ray source SAX J2103.5+4545 was discovered by *BeppoSAX* during its outburst between 1997 February and September with 358.61 s pulsations and a spectrum consistent with an absorbed power-law model with the photon index of $\sim$1.27 and the absorption column density of $\sim$3.1 $\times 10^{22}$ cm^{-2} (Hullemann, in't Zand & Heise 1998).

Starting with the 1999 November outburst detected by the All-Sky Monitor (ASM) on the *Rossi X-ray Timing Explorer (RXTE)*, SAX J2103.5+4545 has been continuously monitored for more than a year through regular pointed *RXTE* observations. From *RXTE* observations, the orbital period and eccentricity of the orbit were found to be 12.68 d and 0.4 (Baykal, Stark & Swank 2000a,b). In the timing analysis, the source was initially found to be spinning up for $\sim$150 d, at which point the flux dropped quickly by a factor of $\simeq$7, and a weak spin-down began afterwards (Baykal et al. 2002). Significant correlation between X-ray flux and spin-up rate was explained by using

the Ghosh & Lamb (1979) accretion disc model. The X-ray spectra well fitted the absorbed power-law model with high energy cut-off and a $\sim$6.4 keV fluorescent emission line (Baykal et al. 2002).

Orbital parameters found by using *RXTE* observations of the source (Baykal et al. 2000a,b) indicated that the source has a high-mass companion. The optical companion of SAX J2103.5+4545 was recently discovered to be a Be-type star with a visual magnitude of $\sim$14.2 (Flippova et al. 2004; Reig et al. 2004).

SAX J2103.5+4545 had another outburst on 2002 July and started to be continuously monitored by *RXTE*. Using $\sim$2 months of *RXTE*-Proportional Counter Array (PCA) observations around the simultaneous coverage of *RXTE* and *XMM–Newton* on 2003 January 6, spin period and spin-up rate of the source were found to be (354.7940 $\pm$ 0.0008) s and (7.4 $\pm$ 0.9) $\times 10^{-13}$ Hz s^{-1} (Inam et al. 2004a). Using this simultaneous coverage, Inam et al. (2004a) discovered 22.7-s quasi-periodic oscillations with a rms fractional amplitude of $\sim$6.6 per cent and a soft spectral component consistent with a blackbody emission with $kT \sim 1.9$ keV and an emission radius of $\sim$0.3 km.

SAX J2103.5+4545 was also observed with the *INTEGRAL* observatory in the 3–200 keV band resulting in a significant detection up to $\sim$100 keV (Lutovinov, Molkov & Revnivtsev 2003; Blay, Reig & Martinez 2004; Flippova et al. 2004; Falanga et al. 2005; Sidoli et al. 2005). The spectral parameters found in the *INTEGRAL*

[*]E-mail: altan@astroa.physics.metu.edu.tr (AB); inam@baskent.edu.tr (SÇİ); starkm@lafayette.edu (MJS); carolyn.heffner@email.ucr.edu (CMH); aerkoca@physics.arizona.edu (AEE); swank@milkyway.gsfc.nasa.gov (JHS)
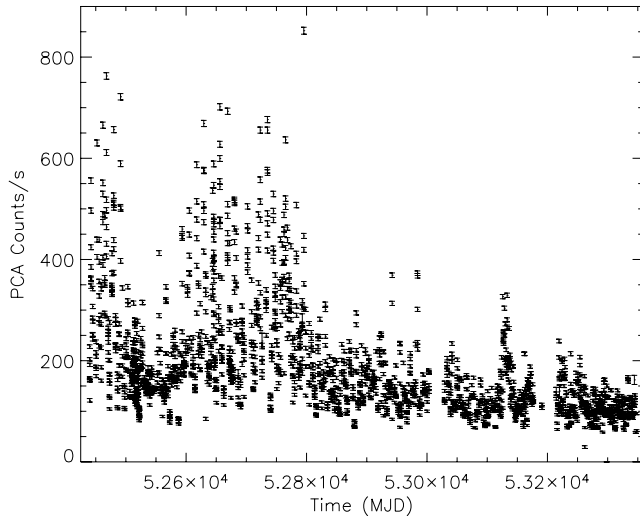
Figure 1. *RXTE*-PCA light curve of SAX J2103.5+4545 after 2002 June outburst of the source.

observations of the source were found to be compatible with those found by Baykal et al. (2002).

2 INSTRUMENT AND OBSERVATIONS

The data set in this paper consists of *RXTE* monitoring observations followed by the 1999 November and 2002 July outbursts of SAX J2103.5+4545. The results presented here are based on data collected with the PCA Jahoda et al. (1996). The PCA instrument consists of an array of five collimated xenon/methane multi-anode proportional counters. The total effective area is approximately 6250 cm^2 and the field of view is ~1^0 full width at half-maximum (FWHM). The nominal energy range extends from 2 to 60 keV. The number of active Proportional Counter Units (PCUs) varied between 1 and 5 during the observations. Observations after 2000 May 13 belong to the observational epoch for which background level for one of the PCUs (PCU0) increased due to the fact that this PCU started to operate without a propane layer. Latest combined background models (CMs) were used together with FTOOLS 6.0 to estimate the appropriate background for timing and spectral analysis.

Results of timing and spectral analysis of all the data after the 1999 outburst were presented before (Baykal et al. 2000a,b, 2002). Inam et al. (2004a) analysed ~2 months part of the data following the 2002 outburst to calculate the spin period and spin-up rate corresponding to the simultaneous *RXTE–XMM–Newton* observations of the source.

In this paper, we extended our timing analysis with the observations after the 2002 outburst. The data after the 2002 outburst have a total exposure of ~650 ks, and span the interval between 2002 July and 2004 December (see Fig. 1). We also analysed the evolution of the X-ray spectrum of the source in this interval.

3 TIMING ANALYSIS

Preliminary timing analysis was performed by folding the light curve on trial periods (Leahy et al. 1983) and producing a chi-square test for each 1-d observation. The period corresponding to the max-

imum chi-square value gives the approximate value of the pulse period of SAX J2103.5+4545. We generated pulse profiles from each *RXTE* observation. Using the orbital parameters, and correcting for light traveltime delays, we also constructed a template pulse profile. We found pulse arrival times by cross-correlating the pulse profiles with the template pulse. In the pulse timing analysis, we used harmonic representation of pulse profiles, which was proposed by Deeter & Boynton (1985). In this method, the pulse profiles for each orbit and the master profile are expressed in terms of harmonic series. We used 10 unweighted harmonic series to cross-correlate the template pulse profile with the pulse profiles for each *RXTE* observation. The maximum value of the cross-correlation is analytically well-defined and does not depend on the phase binning of the pulses.

The source SAX J2103.5+4545 has a variable pulse profile which affects the pulse timing. In order to estimate the errors in the arrival times, the light curve of each *RXTE* observation was sampled into approximately four to five equal subsets, and new arrival times were estimated. The standard deviation of the arrival time delays obtained from each subset of the observation was taken to be the uncertainty of the arrival time of that observation.

The observations were sampled a couple of times per week. Within these time intervals the contribution of pulse frequency derivatives on cycle counts is not significant [i.e. $1 \ll (1/2)\dot{\nu}\Delta t)^2$], therefore we were able to phase connect the pulse arrival times for the data after 1999 November and 2002 June outbursts separately. Since there is a ~450 d gap between these two data sets, we did not phase connect arrival times together. In order to refine the orbital period, we first obtained the orbital epochs ($T_\pi/2$). We divided pulse arrival times into 11 independent subsets. Time series corresponding to each pulse arrival time had a time-span between 36 and 184 d. The arrival time delays may arise from the variations of the pulse frequency and its time derivatives (or intrinsic pulse frequency derivatives) and variations of the orbital parameters (Deeter, Pravdo & Boynton 1981; Boynton et al. 1986).
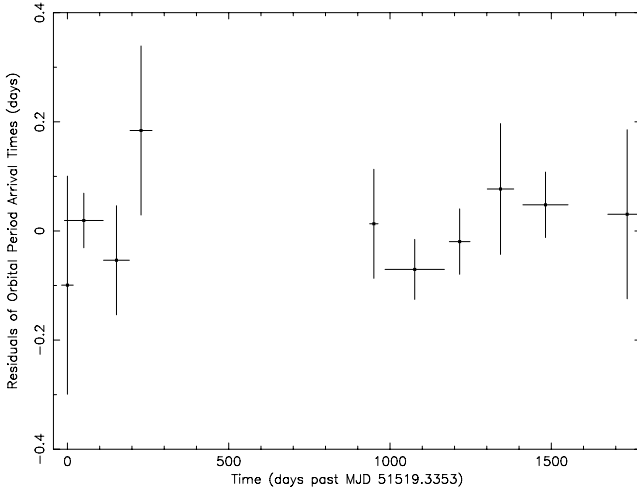
In each interval, we fitted pulse phases ϕ (negative of the pulse arrival times normalized to pulse period) to the Taylor expansion and orbital model,

$$\delta\phi = \delta\phi_o + \delta\nu(t - t_o) + \sum_{n=2}^{5} \frac{1}{n!}\frac{d^n\phi}{dt^n}(t - t_o)^n + f(t_n), \qquad (1)$$

where $\delta\phi$ is the pulse phase offset deduced from the pulse timing analysis, t_o is the mid-time of the each data set, $\delta\phi_o$ is the residual phase offset at t_o, $\delta\nu$ is the correction of pulse frequency at time t_0, $d^n\phi/dt^n$ for $n = 2, 3, 4, 5$ are the first-, second-, third- and fourth-order derivatives of pulse frequency; $f(t_n)$ characterizes the orbital Doppler delay which is parametrized by five Keplerian orbital parameters, projected semimajor axis $a_x/c \sin i$ (where i is the inclination angle between the line of sight and the orbital angular momentum vector), orbital period P_{orb}, eccentricity e, longitude of periastron ω and orbital epoch $T_{\pi/2}$ which is defined when the mean longitude is 90°. We used fifth-order polynomials in the Taylor expansion. The degree of the polynomial is completely arbitrary. We increased the degree of polynomial until we obtained the rms values of phase residuals at the order of uncertainty of the phase estimates (~0.04). We obtained the polynomial-free trends in phase residuals when we removed fifth-order polynomial trend from pulse phases for the time intervals given in Table 1. The time-span of each set depends on pulse frequency fluctuations; for less pulse frequency fluctuations we used longer time-spans of pulse phase data sets.

Table 1. Orbital epochs by pulse timing analysis.

Orbit number	Orbital epoch (MJD)	Time-span (d)	Reference
0	51519.33 ± 0.20	36	Baykal et al. (2000b)
4	51570.11 ± 0.05	120	This work
12	51671.36 ± 0.10	80	This work
18	51747.59 ± 0.15	68	This work
75	52469.35 ± 0.10	26	This work
85	52595.92 ± 0.05	184	This work
96	52735.29 ± 0.05	64	This work
106	52862.04 ± 0.11	82	This work
117	53001.33 ± 0.05	140	This work
137	53254.62 ± 0.15	120	This work

Table 2. Orbital parameters of SAX J2103.5+4545.

Parameter	Value
$T_{\pi/2}$ Orbital epoch (MJD)	52469.336 ± 0.057
$a_x \sin i$ (lt-s)	74.07 ± 0.86
e	0.4055 ± 0.0032
ω(deg)	244.3 ± 6.0
P_{orbit}	12.66536 ± 0.00088

Figure 2. Time delays of arrival times of orbital epochs of SAX J2103.5+4545.

Figure 3. Pulse frequency history of SAX J2103.5+4545.

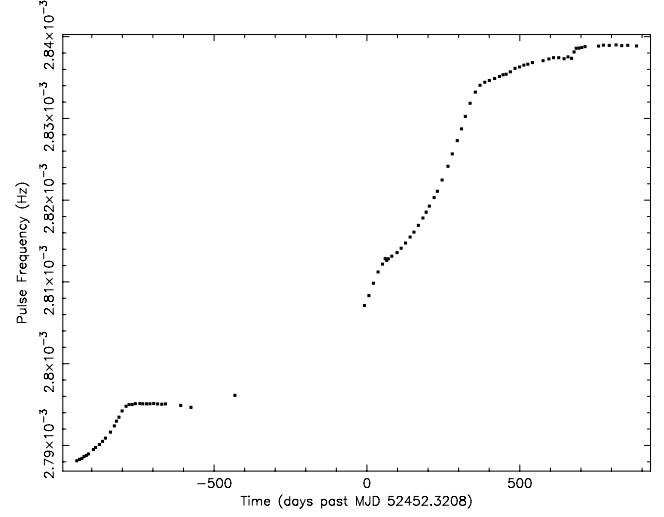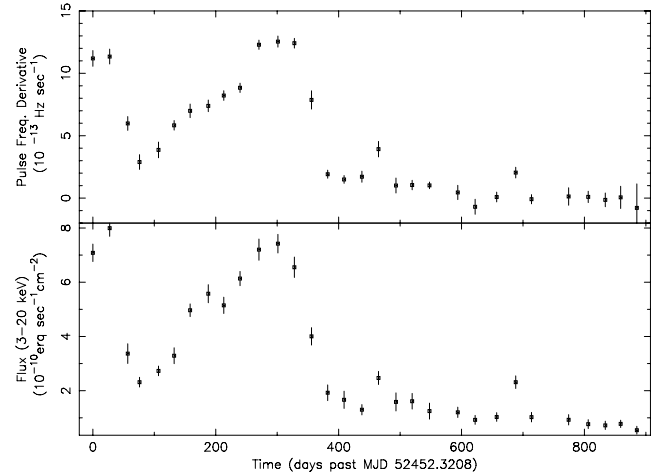**Figure 4.** Pulse frequency derivatives and X-ray flux history of SAX J2103.5+4545.

Then using the $\Delta\chi^2$ method for single parameter estimation, we estimated the orbital epochs in 1σ confidence level (Bevington 1969; Press, Flannery & Teukolsky 1986). In Table 1, we present the orbital epoch measurements and orbital cycle number (n). In Fig. 2, we present observed minus calculated values of orbital epochs ($T_{\pi/2} - n\langle P_{orbit}\rangle - \langle T_{\pi/2} - n\langle P_{orbit}\rangle\rangle$) relative to the constant orbital period ($\langle P_{orbit}\rangle$ = 12.665, 36 d). As seen from Fig. 2, residuals of arrival times of orbital epoch are consistent with a new value, i.e. 12.665 36 d, of constant orbital period. A quadratic fit to the epochs yields an estimate of upper limit for the rate of period change $\dot{P}_{orb}/P_{orb} = \pm1.4 \times 10^{-4}$ yr^{-1}.

Using the constant new orbital period, we fitted pulse phases to orbital parameters $a_x/c \sin i$, eccentricity e and longitude of periastron ω simultaneously for all segments along with an independent orbital epoch $T_{\pi/2}$ and pulse frequency derivatives d$^n\nu$/dt^n, where n = 2, 3, 4, 5 for each segment. In Table 2, we present refined orbital parameters and their uncertainties.

Using this new refined orbital parameters, we regenerated the pulse phases and constructed the pulse frequency time series for all *RXTE*/PCA observations. For the estimation of pulse frequencies, we made linear fits to the phase offsets [$\delta\phi = \phi_0 + \delta\nu (t - t_0)$] with nearly one orbital period resolution. These are presented in Fig. 3. We constructed the pulse frequency derivatives by adding a quadratic term $(1/2)\dot{\nu}(t - t_0)^2$ to the Taylor expansion. We estimated the pulse frequency derivatives from the coefficients of quadratic polynomials. For this purpose, we fitted quadratic polynomial to

phase offsets at two orbital period time resolution shown at the top panel of Fig. 4. From top panel of Fig. 4 (between ∼178 and ∼309 d), our pulse frequency derivative values corresponding to the ∼131 d interval between MJD 52629.9 and MJD 52761.3 are consistent with the previous pulse period derivative measurement using *INTEGRAL* observations (Sidoli et al. 2005).

The bottom panel of Fig. 4 shows the X-ray fluxes associated with the pulse frequency derivatives. These X-ray fluxes were obtained from the spectral analysis of the 3–20 keV PCA data corresponding to the same time intervals that were used to calculate the frequency
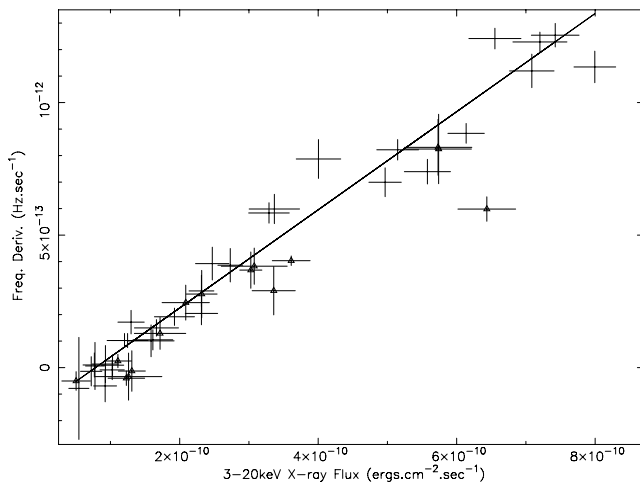
Figure 5. X-ray flux and pulse frequency correlations, the best fit denotes Ghosh–Lamb model. Points denoted by triangles correspond to previous outburst's values found by Baykal et al. (2002).

Figure 6. Power density of pulse frequency derivatives of SAX J2103.5+4545, asterisk denotes the instrumental noise.

derivatives of the source (see next section for the details of our spectral analysis). In Fig. 5, we present the pulse frequency derivatives and X-ray fluxes together with the published values by Baykal et al. (2002). It is seen that, for both outbursts, pulse frequency derivatives are correlated with X-ray flux values.

In order to see the statistical trend of pulse frequency derivatives, we constructed the power spectrum of the pulse frequency derivatives. We used the Deeter polynomial estimator method (Deeter 1984) to derive the power spectrum from the pulse frequency measurements. This technique uses the polynomial estimators instead of sinusoidal estimates for each time-scale T. The power density estimator $P_{\dot{\nu}}(f)$ is defined as $\int_0^\infty P_{\dot{\nu}}(f) = \langle(\dot{\nu} - \langle\dot{\nu}\rangle)^2\rangle$ where $\langle\dot{\nu}\rangle$ means pulse frequency derivative of given analysis frequency. In order to estimate the power density, we first divided the spin frequency measurements into time-spans of duration T and fitted a quadratic polynomial in time. The observed time series was simulated by a Monte Carlo technique for a unit white noise strength defined as $P_{\dot{\nu}}(f) = 1$ and fitted with a quadratic polynomial in time. Then the square of the second-order term was normalized to the value obtained from Monte Carlo simulation (Cordes 1980; Deeter 1984). The logarithmic average of these estimators over the same time intervals is the power density estimate. This procedure was repeated for different durations T to obtain a power spectrum. The power due to instrumental noise was subtracted from the estimates and shown independently by cross symbols. The frequency response of each power density and instrumental noise estimates are presented at $f \sim 1/T$. In Fig. 6, we present power of pulse frequency derivatives $[P_{\dot{\nu}}(f)]$ per Hertz as a function of analysis frequency f. The slope of the power spectrum between 1/1858 and 1/52 d^{-1} yields a power-law index 2.13 ± 0.6. This is the steepest power-law index seen among the HMXRBs (Bildsten et al. 1997). It should also be noted that SAX J2103.5+4545 is the first transient HMXRB for which the noise power spectrum is constructed. The power spectrum indicates that at short time-scales pulse frequency derivative fluctuations are less noisy. On the contrary, at long time-scales, pulse frequency derivative noise strengths are stronger. This could be qualitatively explained by well-defined accretion disc at shorter time-scales possessing low timing noise, therefore power density spectrum becomes more steeper relative the other persistent HMXRBs.
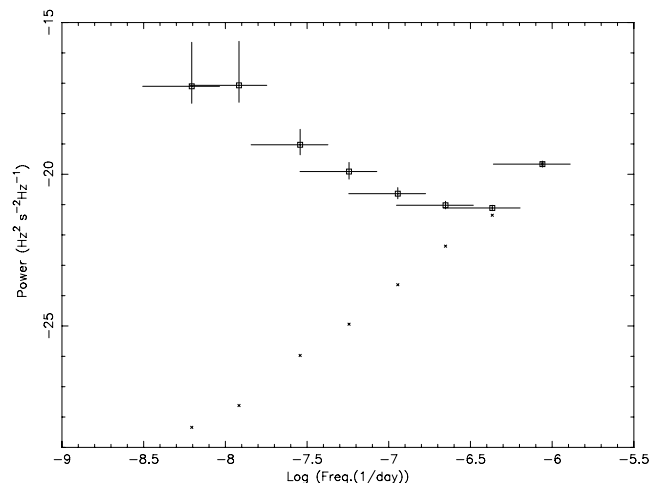
4 SPECTRAL ANALYSIS

We analysed 31 PCA spectra of SAX J2103.5+4545 obtained from data corresponding to the same time intervals that were used to calculate the frequency derivatives shown in Fig. 4.

Spectrum, background and response matrix files were created using FTOOLS 6.0 data analysis software. We used background-subtracted spectra in our analysis. Energy channels corresponding to the 3–20 keV energy range were used to fit the spectra. We ignored photon energies lower than 3 keV due to uncertainties in background modelling, while energies higher than 20 keV were ignored as a result of poor counting statistics. No systematic error was added to the errors.

We fitted the spectra using two models. The first model consists of an absorbed power law (Morrison & McCammon 1983) with a high-energy cut-off (White, Swank & Holt 1983). The second model has an additional soft component modelled as a blackbody using BBODYRAD model in XSPEC software with the peak energy frozen at 1.9 keV. This frozen peak energy is consistent with the previously found value of the soft blackbody component of SAX J2103.5+4545 (Inam et al. 2004a). For both models, an iron line feature at ~6.4 keV was required to fit the spectrum. The first model was previously found to well-fit the X-ray spectrum of SAX J2103.5+4545 for the energies higher than ~3 keV using *RXTE* (Baykal et al. 2002; Inam et al. 2004a), and *INTEGRAL* (Lutovinov et al. 2003; Flippova et al. 2004) observations. Using *XMM–Newton* observations, the second model was found to fit the spectrum better when the energies lower than ~3 keV were included (Inam et al. 2004a).

Our results showed that two spectral models fit almost equally well to the spectrum in 3–20 keV band (see Fig. 7). For the model with the blackbody component, cut-off and e-fold energy parameters were found to vary between ~13.2–17.0 and ~13.3–34.0 keV. For the model without the blackbody component, the same parameters were found to vary between ~6.6–10.9 and ~17.0–45.1 keV.

For the blackbody model, the blackbody normalization was found to vary between ~0.05 and 1.07 km² (10 kpc)⁻². Corresponding blackbody and power-law fluxes were found to be correlated with each other. Thus, the total unabsorbed flux was found to be correlated with the blackbody flux.
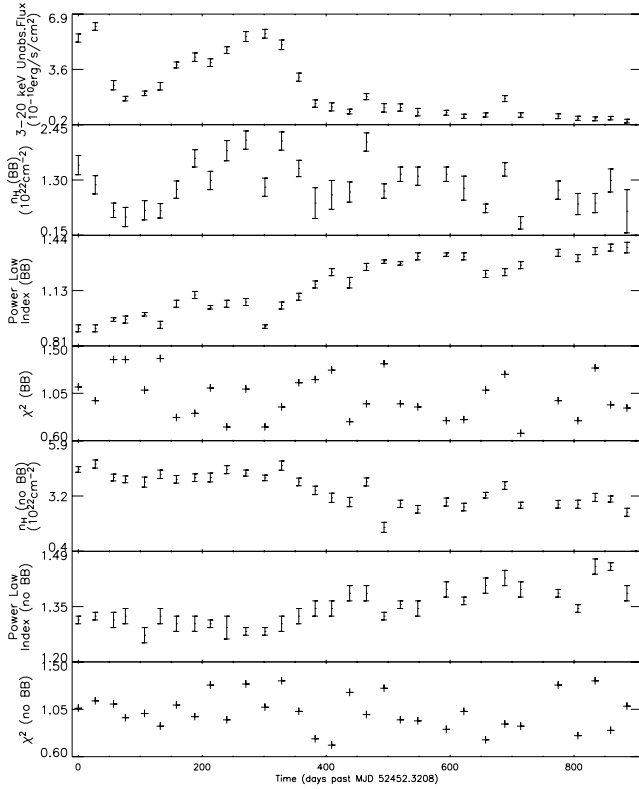
Figure 7. Variation of 3–20 keV unabsorbed flux, hydrogen column density, power-law index and reduced χ^2 for the spectral model with blackbody component, same spectral parameters and reduced χ^2 for the spectral model without blackbody component. For the model with the blackbody component blackbody peak energy and iron linewidth were fixed at 1.9 and 0 keV, respectively.

5 DISCUSSION

A correlation between pulse frequency derivative and X-ray flux has been observed in the outbursts of many X-ray pulsar transient systems. These systems are EXO 2030+375 (Parmar et al. 1989a; Parmar, White & Stella 1989b; Reynolds et al. 1996), 2S 1417−62 (Finger, Wilson & Chakrabarty 1996; Inam et al. 2004b), GRO J1744−28 (Bildsten et al. 1997), XTE J1543−568 (in't Zand, Corbet & Marshall 2001), KS 1947+300 (Morgan et al. 2002; Tsygankov & Lutovinov 2005) and SAX J2103.5+4545 (Baykal et al. 2002). All of these sources have shown correlations between spin-up rate and X-ray flux. Among them, only SAX J2103.5+4545 has been observed to have both spin-up and spin-down episodes. The correlation between spin-up/down and X-ray flux can be explained by accretion from an accretion disc. Both outbursts of SAX J2103.5+4545 started with a spin-up trend, made a transition to a steady spin rate and then appeared to just begin a spin-down trend (see Fig. 4 and Baykal et al. 2002). In Fig. 5, we present the X-ray flux and pulse frequency derivative correlations including the results found in this paper and in Baykal et al. (2002).

If the accretion is via an accretion disc, then the Keplerian rotation of the disc is disrupted by the magnetosphere at the inner disc edge. Then the plasma is forced to accrete along the magnetic field lines.

The inner disc edge r_0 moves inward with increasing mass accretion rate. The dependence of the inner disc edge r_o on the mass accretion rate $\dot{M}$ may approximately be expressed as (Pringle &

Rees 1972; Lamb, Pethick & Pines 1973)

$$r_o = K \mu^{4/7} (GM)^{-1/7} \dot{M}^{-2/7}, \tag{2}$$

where $\mu \simeq BR^3$ is the neutron star magnetic moment with B the magnetic field, R the neutron star radius, G the gravitational constant and M the mass of the neutron star. In this equation, $K = 0.91$ gives the Alfvén radius for spherical accretion. Then the torque estimate is given by Ghosh & Lamb (1979) as

$$2\pi I \dot{\nu} = n(w_s)\dot{M}l_{\mathrm{K}}, \tag{3}$$

where I is the moment of inertia of the neutron star, $l_{\mathrm{K}} = (GM)r_o)^{1/2}$ is the specific angular momentum added by a Keplerian disc to the neutron star at the inner disc edge r_o;

$$n(w_s) \approx 1.4(1 - w_s/w_c)/(1 - w_s) \tag{4}$$

is a dimensionless torque which is a measure of the variation of the accretion torque as estimated by the fastness parameter

$$w_s = \nu/\nu_{\mathrm{K}}(r_o) = (r_o/r_{co})^{3/2} = 2\pi K^{3/2} P^{-1} (GM)^{-5/7} \mu^{6/7} \dot{M}^{-3/7}, \tag{5}$$

where $r_{co} = (GM/(2\pi\nu)^2)^{1/3}$ is the corotation radius at which the centrifugal forces balance the gravitational forces, w_c is the critical fastness parameter at which the accretion torque is expected to vanish. The critical fastness parameter w_c has been estimated to be ~ 0.35 and depends on the electrodynamics of the disc (Ghosh & Lamb 1979; Wang 1987; Ghosh 1993; Li & Wickramasinghe 1998; Torkelsson 1998; Dai & Li 2006).

The accreted material will produce X-ray emission at the neutron star surface with a luminosity expressed as

$$L = \eta GM\dot{M}/R, \tag{6}$$

where $\eta \leqslant 1$ is the efficiency factor. From equations (2), (3) and (6), the rate of spin-up is related to the X-ray intensity through

$$\dot{\nu} \propto n(w_s)L^{6/7} = n(w_s)(4\pi d^2 F)^{6/7}, \tag{7}$$

where d is the distance to the source and F is the X-ray flux.

The distance of the source from optical observations was found to be 6.5 ± 0.9 kpc (Reig et al. 2004, 2005). Although cyclotron emission has not been seen from this source, the hard spectrum and cut-off energy suggest that the magnetic field is greater than 10^{12} Gauss (Lutovinov et al. 2003; Flippova et al. 2004; Falanga et al. 2005; Sidoli et al. 2005). We fitted the Ghosh & Lamb model setting power-law index, magnetic field and distance as a free parameter. We obtained for the distance to the source 4.5 ± 0.5 kpc and for the magnetic field $(16.5 \pm 2.5) \times 10^{12}$ Gauss. We obtained a power-law index 0.96 ± 0.14 which is consistent with the value 6/7 expected in the model. The large uncertainty in this power-law index shows that radiation pressure-dominated accretion disc model with power-law index 0.925 is also possible (see Ghosh 1993). Since the peak outburst luminosity ($\sim 2 \times 10^{36}$ erg s^{-1}, assuming a distance of 4.5 kpc) is far below the Eddington limit ($\sim 10^{38}$ erg s^{-1}), we consider that gas pressure accretion disc with power-law index 6/7 model is the appropriate model for this source. It is also seen in Fig. 5, the points corresponding to spin-up and spin-down are consistent with torque model.

Our distance estimate is lower by $\sim 2\sigma$ than the value obtained from optical observations. The discrepancy could arise from the efficiency factor between accretion X-ray luminosity and observed luminosity. Another factor could be the uncertainty of interstellar absorption coefficient used in optical observations (see Reig et al. 2004, and references therein)

The noise torque fluctuations of accreting X-ray pulsars are subject to both external and internal torques. The external torques arise

from both the accretion of matter from the binary companion and the interaction of the pulsar magnetosphere with accretion disc. The internal torques arise from the response of the neutron star to these external torques and depend on the interior structure of neutron stars. However, due to the pulse shape noise and consequent instrumental noise, torque fluctuations at short time-scales (or analysis frequencies) could not be resolved so far (Baykal, Alpar & Kiziloglu 1991; Baykal 1997). Bildsten et al. (1997) constructed noise power spectra of HMXRBs using BATSE/CGRO pulsar observations. They found that for Vela X-1, Her X-1, 4U 1538-52 and GX 301-2, pulse frequency derivative fluctuations ($P_{\dot\nu}$) are consistent with a white torque noise model. For OAO 1657-415, GX 1+4 and Cen X-3, they showed that red torque noise for which $P_{\dot\nu}$ is proportional to f^{-1}. Our results indicate that for SAX J 2103.5+4545, $P_{\dot\nu}$ is proportional to f^{-2}. In other words, torque fluctuations are characterized as first-order random walk in pulse frequency derivatives. The main reason of this might be the formation of transient accretion discs which leads to the formation of step like torque fluctuations on SAX J2103.5+4545. For higher analysis frequencies of $\sim 1/13\,d^{-1}$, instrumental noise due to the pulse shape fluctuations limits the pulse timing and hence cut-off the torque noise fluctuations.

It was shown for SAX J2103.5+4545 that there is $\sim$50 per cent X-ray flux modulation within the time-span of orbital period at the bright part of observations (see fig. 8 of Baykal et al. 2000b and fig. 4 of Baykal et al. 2002). Assuming that the pulse frequency and X-ray spectra correlations as seen in Fig. 5 are valid at short time-scales in single orbit, we estimate the phase offsets using the Ghosh and Lamb torque model as in $\delta\phi \sim \int\int \dot\nu\,dt \sim \int\int L^{6/7}\,dt \sim 0.0027$. This phase offset corresponds to the $1/0.0027 = 358$ part of pulse phase. Typical uncertainty of pulse phases is $\sim$0.04 which is much larger than the phase offsets of torque fluctuations. Therefore, we could not resolve the torque fluctuations within the orbital period time-scale.

From the X-ray spectral analysis of SAX J2103.5+4545, we found that two spectral models fit almost equally well to data. The first spectral model consisting of absorbed power law with a high-energy cut-off is a typical model for accretion-powered pulsars (White et al. 1983). This spectral model has been found to well fit X-ray spectrum of SAX J2103.5+4545 before (Hullemann et al. 1998; Baykal et al. 2002; Lutovinov et al. 2003; Flippova et al. 2004; Play et al. 2004; Falanga et al. 2005; Sidoli et al. 2005).

The second spectral model has an additional soft component modelled as a blackbody. The model with a soft component was recently found to better fit the X-ray spectrum of SAX J2103.5+4545 when energies lower than 3 keV were included (Inam et al. 2004a). While fitting the spectra using this model, we fixed the blackbody peak energy at 1.9 keV (typical value found by Inam et al. 2004a) since our energy range does not cover around 1.9 keV and large uncertainties of this parameter might have arisen. The blackbody component in accretion-powered pulsars comes either from the reprocessed emission of the surrounding material or from the polar caps of the neutron stars (see Inam et al. 2004a, and references therein). Inam et al. (2004a) found that the polar cap interpretation is more likely for the blackbody emission of SAX J2103.5+4545. For the distance of 4.5 kpc and considering the variation of the blackbody normalization, we estimated the radius of blackbody emitting region to be varying between $\sim$0.01 and 0.47 km which is consistent with $\sim$0.3 km value found by Inam et al. (2004a).

For both of the spectral models, we found that power-law index anticorrelates with the unabsorbed X-ray flux (see Fig. 7). This anticorrelation indicates that the spectrum gets softer with the decreasing X-ray flux. This anticorrelation was previously found in

the data set after the 1999 outburst of SAX J2103.5+4545 (Baykal et al. 2002), and in the data set after the 1999 outburst of 2S 1417-62 (Inam et al. 2004b). This type of spectral softening accompanied with decreasing flux was found to be primarily a consequence of mass accretion rate change and is not necessarily related to a significant accretion geometry change (Meszaros et al. 1983; Harding et al. 1984).

ACKNOWLEDGMENTS

REFERENCES

Baykal A., 1997, A&A, 319, 515
Baykal A., Alpar A., Kiziloglu U., 1991, A&A, 252, 664
Baykal A., Stark M., Swank J., 2000a, IAU Circ. 7355
Baykal A., Stark M., Swank J., 2000b, ApJ, 544, L129
Baykal A., Stark M., Swank J., 2002, ApJ, 569, 903
Bevington P. R., 1969, Data Reduction and Error Analysis for the Physical Sciences. McGraw-Hill, New York
Bildsten L. et al., 1997, ApJS, 113, 367
Blay P., Reig P., Martinez Nunez S., Camero A., Connell P., Reglero V., 2004, A&A, 427, 293
Boynton P. E., Deeter J. E., Lamb F. K., Zylstra G., 1986, ApJ, 307, 545
Cordes J. M., 1980, ApJ, 237, 216
Dai H.-L., Li X.-D., 2006, A&A, 451, 581
Deeter J. E., 1984, ApJ, 281, 482
Deeter J. E., Boynton P. E., 1985, in Hayakawa S., Nagase F., eds, Proc. Inuyama Workshop on Timing Studies of X-Ray Sources. Nagoya Univ., Nagoya, p. 29
Deeter J. E., Pravdo S. H., Boynton P. E., 1981, ApJ, 247, 1003
Falanga M. et al., 2005, A&A, 436, 313
Flippova E. V., Lutovinov A. A., Shtykovsky P. E., Revnivtsev M. G., Burenin R. A., Arefiev V. A., Pavlinsky M. N., Sunyaev R. A., 2004, Astron. Lett., 30, 824
Finger M. H., Wilson R. B., Chakrabarty D., 1996, A&AS, 120, 209
Ghosh P., 1993, in Holt S. S., Day C. S., eds, The Evolution of X-ray Binaries. Am. Inst. Phys., New York, p. 439
Ghosh P., Lamb F. K., 1979, ApJ, 234, 296
Harding A. K., Kirk J. G., Galloway D. J., Meszaros P., 1984, ApJ, 278, 369
Hullemann F., in't Zand J. J. M., Heise J., 1998, ApJ, 337, L25
Inam S. C., Baykal A., Swank J., Stark M. J., 2004a, ApJ, 616, 463
Inam S. C., Baykal A., Scott D. M., Finger M., Swank J., 2004b, MNRAS, 349, 173
in't Zand J. J. M., Corbet R. H. D., Marshall F. E., 2001, ApJ, 553, L165
Jahoda K., Swank J., Giles A. B., Stark M. J., Strohmayer T., Zhang W., Morgan E. H., 1996, Proc. SPIE, 2808, 59
Lamb F. K., Pethick C. J., Pines D., 1973, ApJ, 184, 271
Leahy D. A., Darbro W., Elsner R. F., Weisskopf M. C., Kahn S., Sutherland P. G., Grindlay J. E., 1983, ApJ, 266, 160
Li J., Wickramasinghe D. T., 1998, MNRAS, 300, 1015
Lutovinov A. A., Molkov S. V., Revnivtsev M. G., 2003, Astron. Lett., 29, 713
Meszaros P., Harding A. K., Kirk J. G., Galloway D. J., 1983, ApJ, 266, 33
Morgan E., Galloway D. K., Chakrabarti D., Levine A. M., 2002, A&AS, 201, 5401
Morrison R., McCammon D., 1983, ApJ, 270, 119
Parmar A. N., White N. E., Stella L., Izzo C., Ferri P., 1989a, ApJ, 338, 359
Parmar A. N., White N. E., Stella L., 1989b, ApJ, 338, 373
Press W. H., Flannery B. P., Teukolsky S. A., 1986, Numerical Recipes. The Art of Scientific Computing. Cambridge Univ. Press, Cambridge
Pringle J. E., Rees M. J., 1972, A&A, 21, 1

Reig P., Negueruela I., Fabregat J., Chato R., Blay P., Mavromatakis F., 2004, A&A, 421, 673

Reig P., Negueruela I., Papamastorakis G., Manousakis A., Kougenakis T., 2005, A&A, 440, 637

Reynolds A. P., Parmar A. N., Stollberg M. T., Verbunt F., Roche P., Wilson R. B., Finger M. H., 1996, A&A, 312, 872

Sidoli L. et al., 2005, A&A, 440, 1033

Torkelsson U., 1998, MNRAS, 298, 55

Tsygankov S. S., Lutovinov A. A., 2005, Astron. Lett., 31, 88

Wang Y.-M., 1987, A&A, 183, 257

White N. E., Swank J. H., Holt S. S., 1983, ApJ, 270, 711

This paper has been typeset from a TEX/LATEX file prepared by the author.